7. D. D. Reible, *J. Hazard Mater.* **37**, 431 (1994). About 20% of the MeBr produced worldwide is used to fumigate structures and shipments of fruits and vegetables.
8. J. H. Butler, *Geophys. Res. Lett.* **21**, 185 (1994); and see (*5*). A more accurate relation between sources, sinks, and lifetime of MeBr can be obtained from a model that treats northern and southern hemispheres separately; see, for example, Khalil *et al.* in (*3*) who also report a 3% per year increase of atmospheric MeBr between 1988–92.
9. K. Yagi, J. Williams, N.-Y. Wang, R. J. Cicerone, *Proc. Natl. Acad. Sci. U.S.A.* **90**, 8420 (1993).
10. Injection rates were metered continuously, and the total amount applied (323 kg/ha = 288 lbs/acre) was also determined to within 1% by weighing the fumigant supply tanks before and after fumigation. The fluid mixture was injected with a Noble-plow design injector to a depth of 35 cm. This injector is configured so that the lines of injection are not directly beneath the furrows caused by plow shanks. Standard plow shanks, in contrast, may facilitate escape of MeBr, as the lines of injected liquid are directly beneath the furrows.
11. The tarp material was high-density polyethylene, nominally 0.025 mm thick (0.001 inch). The actual thicknesses of the sections beneath our flux chambers were between 0.035 and 0.042 mm.
12. Soil sampling at 10, 20, 30, 60, and 90 cm was achieved as in (*9*) but also with a second set of new sampling tubes at each location. The new tubes were of low dead volume and were placed inside a stainless steel main tube with an outer diameter of 1.27 cm that had solid disks fused inside at each sampling depth. Each individual sampling tube connected to holes drilled into its disk, and the other tubes passed through the disk to greater depths. Flame ionization gas chromatography was used to measure MeBr as in (*9*).
13. The electrodes were manufactured by Orion Research, Boston. Air-dried soil samples (25 g, diameters <2 mm) were treated with 50 ml of 0.4 M $NaNO_3$ to extract bromide. Calibration was by NaBr solutions (0.1, 1, and 10 parts per million) prepared in 0.4 M $NaNO_3$. Samples from three locations about 1.5 m apart were combined for surface soil and for the depths of 10, 20, and 30 cm; samples from two such sites were used for the 60- and 90-cm depths. Bromide concentrations measured before and after MeBr II are shown in Fig. 3. Bromide amounts before MeBr I were measured to be 1.65 μg/g at 3 cm and assumed to be the same down to 60 cm, and to increase linearly to 4.64 μg/g at 90 cm (the same value that was observed at the end of MeBr I). Comparison with measurements after MeBr I implied that there was an increase of 4.09 g of Br^- per square meter during the 7-day experiment, or 19% of the applied bromine.
14. We observed smaller fluxes when we made additional flux measurements from those parallel strips where adjacent tarp sheets overlapped. We accounted for this effect by using area-weighted flux values for the part of the field (93%) that was covered by a single thickness of tarp and the 7% covered by double-thick tarp. We also found negligible fluxes from unfumigated areas horizontally adjacent to the fumigated field.
15. Vertical profiles of gaseous MeBr were reported in (*9*) for the duration of MeBr I. In the present experiment, MeBr II, we measured vertical profiles in even more detail but do not include the results here.
16. P. Hamaker, H. de Heer, A. M. M. van der Burg, *Acta Hortic.* **152**, 127 (1983).
17. I. A. Gentile, L. Ferraris, S. Crespi, *Pestic. Sci.* **25**, 261 (1989). In our own laboratory experiments with several soils (to be reported elsewhere) we also found bromide production from MeBr to be about 35% faster with pH 6.9 than for pH 6.1.

18. Discussions with T. Duafala and D. Ito of TriCal and access to fields professionally fumigated by TriCal are appreciated. Supported by NSF grant ATM-9321867 and Department of Energy National Institute for Global Environmental Change award W-GEC91-089-UCI.

8 October 1994; accepted 30 January 1995

Signatures of the Martian Atmosphere in Glass of the Zagami Meteorite

K. Marti,* J. S. Kim,† A. N. Thakur, T. J. McCoy,‡ K. Keil§

Isotopic signatures of nitrogen, argon, and xenon have been determined in separated millimeter-sized pockets of shock-melted glass in a recently identified lithology of the meteorite Zagami, a shergottite. The ratio of nitrogen-15 to nitrogen-14, which is at least 282 per mil larger than the terrestrial value, the ratio of xenon-129 to xenon-132 = 2.40, and the argon isotopic abundances match the signatures previously observed in the glassy lithology of the Antarctic shergottite EETA 79001. These results show that the signatures in EETA 79001 are not unique but characterize the trapped gas component in shock-melted glass of shergottites. The isotopic and elemental ratios of nitrogen, argon, and xenon closely resemble the Viking spacecraft data for the martian atmosphere and provide compelling evidence for a martian origin of the two shergottites and, by extension, of the meteorites in the shergottites-nakhlites-chassignites (SNC) group.

The SNC group of igneous meteorites is derived from a parent body with an oxygen isotopic signature that is distinct from that of other solar system objects (*1*). The crystallization ages of these meteorites, although the subject of some debate, are clearly less than 1.3×10^9 years, possibly as low as 180×10^6 years (*2*), and must have formed on a geologically complex parent body (*3*). Bogard and Johnson (*4*) and Becker and Pepin (*5*) discovered that trapped noble gases and nitrogen in lithology C of the Antarctic shergottite EETA 79001 had elemental and isotopic ratios similar to those measured by the Viking lander (*6*) in the martian atmosphere, lending support to the suggestion that these meteorites may have come from Mars. The shergottite EETA 79001 remains the only shergottite that shows clear signatures of entrapped martian atmospheric gases (*7*). Recently, Watson *et al.* (*8*) studied the hydrogen isotopic signatures in Zagami and other SNC meteorites and found high deuterium/hydrogen (D/H) ratios, which are similar to that measured in the martian atmosphere by Earth-based telescopes (*9*).

In this work, we present the results of the first petrographic and isotopic studies on the shock-melted glasses in Zagami. Zagami was selected for study because it probably crystallized near the surface of Mars (*10*) and thus is in close proximity to the source of the implanted atmospheric gases. Zagami is also a recent fall (1962), and the degree of terrestrial contamination was expected to be less severe than in the Antarctic shergottite EETA 79001. Multimillimeter-sized pockets of shock-melt suitable for separation and isotopic analyses are not evenly distributed in Zagami. Most of Zagami (~80%) has a basaltic lithology (*10, 11*), termed "normal Zagami," in which shock-melting is evident only because of the presence of ~100-μm-wide shock-melt veins of roughly whole-rock composition that cross-cut the sample (*10*). These veins are too small for separation and isotopic analyses. A second, recently recognized lithology occupies ~20% of Zagami and is termed the "dark, mottled lithology" (*12*). It is enriched in late-stage crystallization product and represents a later stage in the crystallization of Zagami. It is within this lithology that we find the multimillimeter-sized shock-melt pockets separated for isotopic analyses.

Two shock-melt pockets were selected for study: one for petrographic examination from samples provided by R. Haag (Fig. 1) and one for isotopic analyses from U.S. National Museum sample 6545. Both pockets were ~3 mm in diameter, much smaller than the centimeter-sized pockets studied from EETA 79001. Like those in EETA 79001, the bulk composition of the petrographically examined shock-melt pockets in Zagami is similar in composition to the bulk lithology in which it occurs. The Zagami pockets differ from the EETA 79001 pockets (*13*) in being enriched in some incompatible elements (for example, Fe, P), reflecting the enrichment of these elements in the "dark mottled lithology" of Zagami. Both pockets have irregular outlines, including embayments into the host, but

K. Marti and J. S. Kim, Department of Chemistry and Biochemistry, University of California at San Diego, La Jolla, CA 92093, USA.
A. N. Thakur, California Space Institute, Scripps Institute of Oceanography, University of California at San Diego, La Jolla, CA 92093, USA.
T. J. McCoy and K. Keil, Hawaii Institute of Geophysics and Planetology, School of Ocean and Earth Science and Technology, University of Hawaii at Manoa, Honolulu, HI 96822, USA.

*To whom correspondence should be addressed.
†Present address: Division of Chemistry and Radiation, Korea Research Institute of Standards and Science, Post Office Box 102, Yusong Taejon, Korea 305-600.
‡Present address: Code SN4, National Aeronautics and Space Administration Johnson Space Center, Houston, TX 77058, USA.
§Also associated with the Hawaii Center for Volcanology, University of Hawaii of Manoa, Honolulu, HI 96822, USA.

there is no evidence that they are attached to any veins and they probably formed in situ. Both Zagami pockets are black and vitreous in hand sample, indicative of their glassy nature. However, petrographic examination (Fig. 1) reveals abundant, incompletely digested, heavily shocked pyroxene grains, similar to shock-melt pockets in EETA 79001 (*13*). Thus, shock-melting was incomplete in both of these meteorites. Also found in the Zagami pockets were small pyroxenes and opaque minerals that appear to have crystallized from the melt. Both pockets in Zagami exhibit vesicles. In the petrographically studied pocket (Fig. 1), the glass defines roughly three-quarters of a large, central vesicle. Shock-melt pockets in EETA 79001 are also described as vesicular (*13*). Thus, shock-melt pockets in Zagami and EETA 79001 appear to be very similar, with the exceptions that the Zagami pockets are smaller and occur only in the later-crystallizing lithology. These similarities are not surprising in light of the similar shock histories experienced by these two meteorites (*14*), with equilibrium shock pressures of 34 ± 1 GPa for EETA 79001 and 29 ± 1 GPa for Zagami.

A single ~22-mg glass chip (sample A) was obtained, and in the same cavity area below the glass chip, additional pockets of glass were removed and combined into an additional glass sample (sample B). A chip of the normal Zagami lithology was also studied for reference purposes. We analyzed all samples for nitrogen, argon, and xenon, using stepped heating procedures by a combination of pyrolysis and combustion steps, the latter in pure O_2 at 5 torr. Isotopic analysis was carried out by static mass spectrometry of separated gases.

The trapped heavy noble gases as well as radiogenic ^{40}Ar and ^{129}Xe are enriched in the glass by an order of magnitude relative to normal Zagami (Table 1). The trapped component in glass is released chiefly at the melting temperature; in contrast, normal Zagami contains a nitrogen component that is released at low temperatures and has isotopic signatures similar to terrestrial nitrogen (Table 1). This may be indicative of a contaminating phase of terrestrial origin rather than indigenous nitrogen. In contrast to normal Zagami, both glass samples contain heavy nitrogen compared with terrestrial nitrogen. The heaviest nitrogen was released in the 1200°C fraction after the glass melted (Fig. 2). Data for glass samples A and B (normalized to equal temperature steps) are internally consistent and reveal a two-component mixture of nitrogen with an approximately terrestrial isotopic signature (dominating at low temperature) and indigenous nitrogen with $\delta^{15}N \geq 325$ per mil (*15*). The isotopic composition of the latter component represents a lower limit because we cannot exclude contributions of the former component in the melt fraction. Moreover, the exposure age of Zagami (3 million years) (*16*, *17*) necessitates consideration of the cosmic-ray–produced spallation $^{15}N_c$ component, which is part of the indigenous Zagami nitrogen. Using a nomi-

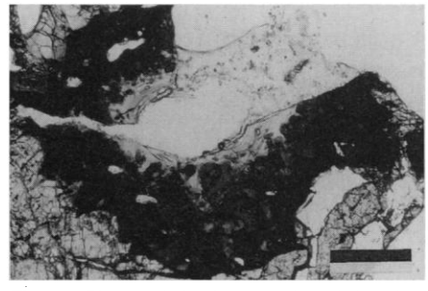

Fig. 1. Plane-polarized, transmitted-light photomicrograph of shock-melt pocket 5 in Zagami. The upper right portion of the pocket was lost during cutting. The pocket shows a textural gradation from a microcrystalline matrix with heavily shocked undigested pyroxene grains at the edge to a clear, highly turbid, opaque-free glass in the center. The turbid glass outlines roughly three quarters of an ovoid vesicle that may once have contained gases generated during shock-melting. Scale bar, 500 μm.

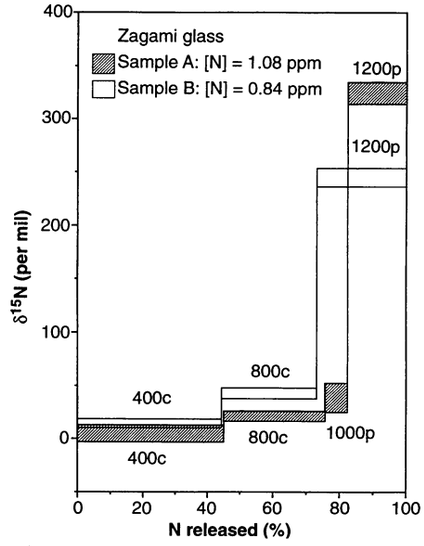

Fig. 2. Nitrogen isotopic signatures (*15*) versus the amount of nitrogen released for Zagami glass samples A and B (c indicates combustion steps; p indicates pyrolysis steps).

Table 1. Isotopic abundances of N, Ar, and Xe in Zagami. The uncertainties in the concentrations are ~7%.

Temperature (°C)	Nitrogen (ppm)	$\delta^{15}N$ (per mil)	^{36}Ar (10^{-9} cm^3 g^{-1})	$^{40}Ar/^{36}Ar$	$^{38}Ar/^{36}Ar$	^{132}Xe (10^{-12} cm^3 g^{-1})	$^{129}Xe/^{132}Xe$
			Zagami glass sample A (21.71 mg)				
400c*	0.476	3.4 ± 12.7	1.05	437 ± 44	0.290 ± 0.003	1.30	1.59 ± 0.20
800c	0.323	21.1 ± 9.3	2.95	1596 ± 160	0.286 ± 0.003	1.29	1.98 ± 0.22
1000p*	0.070	38.6 ± 27.3	3.57	1226 ± 123	0.334 ± 0.007	0.92	1.97 ± 0.20
1200p	0.188	324.6 ± 20.2	31.9	1538 ± 154	0.317 ± 0.001	28.86	2.40 ± 0.08
1500p	0.019		1.37	124 ± 3	0.468 ± 0.013	0.47	
Total	1.076	68.2	40.8	1439	0.321	32.84	2.35
			Zagami glass sample B (18.92 mg)				
400c	0.370	14.3 ± 8.4	3.14	637 ± 37	0.289 ± 0.001	1.42	1.40 ± 0.27
800c	0.240	42.9 ± 10.2	3.26	1716 ± 172	0.269 ± 0.002	2.29	1.90 ± 0.13
1200c	0.226	244.7 ± 17.4	28.10	1532 ± 153	0.319 ± 0.003	30.37	2.31 ± 0.05
1500p	0.008		1.71	350 ± 12	0.553 ± 0.024	2.38	2.19 ± 0.12
Total	0.844	94.7	36.2	1415	0.323	36.46	2.24
			Zagami normal (56.9 mg)				
400c	16.51	0.8 ± 1.4	0.50	279 ± 79	0.860 ± 0.414	0.74	1.27 ± 0.11
800c	5.65	3.9 ± 4.8	0.55	1760 ± 185	0.485 ± 0.186	0.16	1.03 ± 0.10
1200p	0.26	16.6 ± 11.9	1.93	673 ± 53	0.688 ± 0.151	2.42	1.38 ± 0.06
1500p	0.009		1.40	171 ± 1	1.279 ± 0.007	1.55	1.74 ± 0.08
Total	22.4	2.05	4.38	604	0.871	4.87	1.47

*Symbols c and p indicates combustion or pyrolysis, respectively.

nal spallation ^{15}N correction based on the exposure age and a meteoritic production rate $P(^{15}N) = 11.6$ pg per million years per gram (*18*), we obtain $\delta^{15}N \geq 282$ per mil for Zagami sample A ≥ and 205 per mil for Zagami sample B. Therefore, spallation-corrected $\delta^{15}N$ values in the Zagami glasses are in good agreement with the range of $\delta^{15}N$ values reported in EETA 79001, lithology C (*5*, *19*).

During the stepwise heating of sample A, the $^{129}Xe/^{132}Xe$ ratio increased from a value of 1.6 at 400°C to 2.4 at the melting temperature, when >80% of the Xe is released (Table 1). The data for sample B are similar. The results indicate the presence of a two-component mixture, with the major component ($^{129}Xe/^{132}Xe \geq 2.4$) dominating the release in the melt fraction. Swindle *et al.* (*20*) also reported a $^{129}Xe/^{132}Xe$ ratio of ≈ 2.4 in EETA 79001, lithology C. The other component may represent the order of magnitude smaller Xe component in normal Zagami, which reveals a low $^{129}Xe/^{132}Xe$ ratio of 1.03 in the 800°C step. We observed higher ratios in other temperature steps of normal Zagami, which signal the presence of small amounts of entrapped Xe.

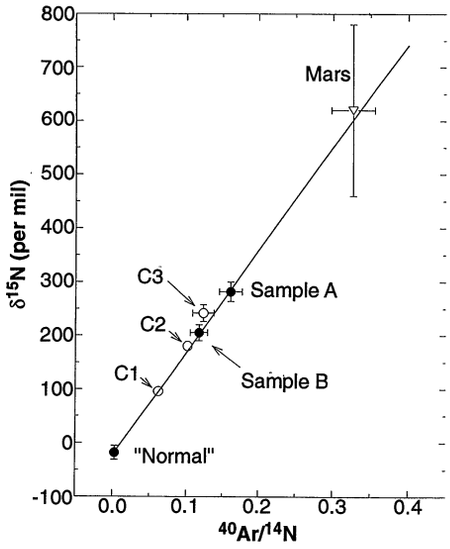

Fig. 3. Linear array of the spallation-corrected $\delta^{15}N$ data in the melt fraction of glass samples A and B and normal Zagami plotted versus their atomic $^{40}Ar/^{14}N$ ratios. This linear array may be interpreted as a mixing line between normal Zagami and "Viking Mars" signatures. For reference, the data for C 1, C 2, and C 3 from EETA 79001, lithology C (*5, 19*) are shown. The Mars atmosphere point represents data from the Viking lander (*6*).

The $^{40}Ar/^{36}Ar$ ratios in both glass samples in the temperature interval from 400° to 1200°C are in the range 1500 to 1700 (Table 1). These ratios are little affected by the presence of in situ radiogenic ^{40}Ar because the total ^{40}Ar observed in normal Zagami is 1/20 of that of ^{40}Ar in the glass. The $^{40}Ar/^{36}Ar$ ratios ≈ 1600 in Zagami glass are at the low end of the range reported for EETA 79001, lithology C (*4*, *5*, *20*). All trapped gas components were modified by the addition of spallogenic gases during the 3×10^6 years that the sample was exposed to cosmic rays. The measured $^{38}Ar/^{36}Ar$ ratios (Table 1), which reveal another interesting signature of trapped argon, can be analyzed into trapped (t) and cosmic-ray–produced (c) components if standard procedures of adopting signatures for the end-members are followed. Calculations based on the use of observed ratios in meteorites of $(^{38}Ar/^{36}Ar)_t = 0.19$ and $(^{38}Ar/^{36}Ar)_c = 1.55$ yielded dissimilar amounts for the cosmic-ray–produced component in Zagami glasses [$^{38}Ar_c = 5.0 \times 10^{-9}$ cm^3 g^{-1} at standard temperature and pressure (STP)] and in normal Zagami ($^{38}Ar_c = 3.0 \times 10^{-9}$ cm^3 g^{-1} at STP), which conflict with the evidence for a similar chemical composition. However, similar $^{38}Ar_c$ concentrations are obtained with a ratio $(^{36}Ar/^{38}Ar)_t \approx 4$. Arguments were presented (*19*, *20*) for the presence of a distinct trapped Ar component in the glassy lithology C of shergottite EETA 79001, with a signature $(^{36}Ar/^{38}Ar)_t = 4.1 \pm 0.2$, and our data agree.

In Fig. 3, the spallation-corrected $\delta^{15}N$ values are plotted against the observed atomic $^{40}Ar/^{14}N$ ratios in the melt fraction of normal Zagami and of glass samples A and B, a correlation used by Becker and Pepin (*5*). The extended fit to the three Zagami data points shows a similarity to the Viking lander Mars data. The data for EETA 79001, lithology C (samples 1, 2, and 3) (*5*, *19*) plot very close to this line, which was interpreted to be a mixing line of indigenous crustal gases with atmospheric gases (*19*).

Many SNC meteorites do not contain unadulterated noble gases (*20*, *21*) or N (*22*) with the signature of the martian atmosphere. Why do only some of the SNC meteorites carry such gases? High shock pressures, local melting, and ambient atmospheric gases (near-surface environments) appear to be required for the shock-loading process. The presence of shock-melt pockets in both Zagami and EETA 79001 indicates local pressure excursions in excess of 80 GPa (*14*). At such pressures, ambient heavy noble gases and N_2 are emplaced into powdered and, with lower efficiency, unpowdered basalt samples (*23*, *24*). Three shergottites are considered to represent near-surface rocks. Two of these (Zagami and EETA 79001) are now known to contain Mars-type gases, whereas the third (Shergotty) shows in bulk rock analyses a gas component with a similar signature (*20*, *21*).

In Table 2 the observed signatures in Zagami glass are compared to those from EETA 79001, lithology C, the atmosphere of Mars, the atmosphere of Earth, and the sun (Earth and sun are listed for reference). The agreement between the Zagami glass data and the data of lithology C in EETA 79001 is excellent. The results from shergottite EETA 79001 suggested a close association between the trapped gases in the shocked lithology C and those observed in the atmosphere of Mars (*4*, *5*, *16*, *19*, *20*, *24*) and led many workers to consider a martian origin for SNC meteorites. This association is now observed in a second shergottite and indicates a general characteristic of shock-melt glasses in shergottites. This strengthens the case for their origin from Mars..

Table 2. Summary of observed isotopic signatures.

Signature	Zagami (glass)	EETA 79001 (lithology C)	Atmosphere of		
			Mars	Earth	Sun
$\delta^{15}N$ (per mil)	≥282 (this work)	≥242 (*19*)	620 ± 160† (*6*)	≡ 0	40‡ (*25*)
$^2H/^1H$ (×10^4)	6.8–8.1* (*8*)		7.6 (*9*)	1.5	≤0.03§ (*26*)
$^{129}Xe/^{132}Xe$	2.40 ± 0.08 (this work)	2.23; 2.4 ±0.04 (*5*, *20*)	$2.5^{+2.0}_{-1.0}$ (*6*)	0.983	1.04‖ (*27*)
$^{40}Ar/^{36}Ar$	1600 ± 100 (this work)	2370; 1660 ±100 (*5*, *20*)	3000 ± 500 (*6*)	296	≈ 0
$^{38}Ar/^{36}Ar$	~0.25 (this work)	0.24 ± 0.01 (*19*)	0.14–0.25 (*28*)	0.188	0.19‖ (*27*)
$^{132}Xe/^{36}Ar$ (×10^3)	1.0 ± 0.2 (this work)	1.43 ± 0.14 (*5*, *20*)	1–10 (*6*)	0.75	0.015 (*29*)
$^{14}N/^{36}$ Ar (×10^{-3})	≤15 (this work)	≤22 (*5*, *20*)	11 ± 3 (*6*)	50	0.037 (*29*)

*Measured in apatite. †Measured at an altitude of 125 km above Mars. ‡Recent solar wind signature. §Lunar soil. ‖Solar type.

REFERENCES AND NOTES

1. R. N. Clayton, *Annu. Rev. Earth Planet. Sci.* **21**, 115 (1993).
2. E. Jagoutz, *Geochim. Cosmochim. Acta* **53**, 2429 (1989).
3. D. Walker, E. M. Stolper, J. F. Hays, *Lunar Planet Sci.* **X**, 1274 (1979); J. T. Wasson and G. W. Wetherill, in *Asteroids*, T. Gehrels, Ed. (Univ. of Arizona

Press, Tucson, 1979), pp. 926–924; C. Y. Shih *et al.*, *Geochim. Cosmochim. Acta* **46**, 2323 (1982); G. Dreibus *et al.*, *Lunar Planet. Sci.* **XIII**, 186 (1982); N. Nakamura, H. Komi, H. Kagami, *Meteoritics* **17**, 257 (1982); H. Y. McSween, *ibid.* **29**, 757 (1994).
4. D. D. Bogard and P. Johnson, *Science* **221**, 651 (1983).
5. R. H. Becker and R. O. Pepin, *Earth Planet. Sci. Lett.* **69**, 225 (1984).
6. A. O. Nier and M. B. McElroy, *J. Geophys. Res.* **82**, 4341 (1977); T. Owen and K. Biemann, *Science* **193**, 801 (1976); T. Owen *et al.*, *J. Geophys. Res.* **82**, 4635 (1977).
7. Noble gas signatures in whole-rock samples of shergottites show only slight excesses of ^{40}Ar and ^{129}Xe (*16, 20, 21*), and a shock-melt glass from LEW 88516 revealed excesses of ^{40}Ar and ^{129}Xe, with no associated heavy N (*22*).
8. L. L. Watson, I. D. Hutcheon, S. Epstein, E. M. Stolper, *Science* **265**, 86 (1994).
9. T. Owen, J. P. Maillard, C. de Bergh, B. L. Lutz, *ibid.* **240**, 1767 (1988).
10. T. J. McCoy, G. J. Taylor, K. Keil, *Geochim. Cosmochim. Acta* **56**, 3571 (1992).
11. E. Stolper and H. Y. McSween, *ibid.* **43**, 1475 (1979).
12. M. Wadhwa, T. J. McCoy, K. Keil, G. Crozaz, *Meteoritics* **28**, 453 (1993).
13. H. Y. McSween and E. Jarosewich, *Geochim. Cosmochim. Acta* **47**, 1501 (1983).
14. D. Stoeffler *et al.*, *ibid.* **50**, 889 (1986).
15. $\delta^{15}N$ (per mil) = 1000 $\{[(^{15}N/^{14}N)_{sample}/(^{15}N/^{14}N)_{Earth\ atm}]-1\}$.
16. D. D. Bogard, L. E. Nyquist, P. Johnson, *Geochim. Cosmochim. Acta* **48**, 1723 (1984).
17. O. Eugster, *Meteoritics* **29**, 464 (1994).
18. J. S. Kim, Y. Kim, K. Marti, *Lunar Planet Sci.* **XXV**, 701 (1994); in preparation.
19. R. C. Wiens, R. H. Becker, R. O. Pepin, *Earth Planet. Sci. Lett.* **77**, 149 (1986).
20. T. D. Swindle, M. W. Caffee, C. M. Hohenberg, *Geochim. Cosmochim. Acta* **50**, 1001 (1986).
21. U. Ott, *ibid.* **52**, 1937 (1988).
22. R. H. Becker and R. O. Pepin, *Meteoritics* **28**, 637 (1993).
23. D. D. Bogard, F. Hörz, P. H. Johnson, *J. Geophys. Res.* **91**, E99 (1986).
24. R. C. Wiens and R. O. Pepin, *Geochim. Cosmochim. Acta* **52**, 295 (1988).
25. J. S. Kim *et al.*, in preparation.
26. S. Epstein and H. P. Taylor, *Geochim. Cosmochim. Acta Suppl.* **2**, 1421 (1971).
27. J. S. Kim and K. Marti, *Lunar Planet Sci.* **XXII**, 145 (1992).
28. K. Biemann, T. Owen, D. R. Rushneck, A. L. LaFleur, D. W. Howarth, *Science* **194**, 76 (1976).
29. E. Anders and N. Grevasse, *Geochim. Cosmochim. Acta* **53**, 197 (1989).
30. We thank G. J. MacPherson and R. Haag for providing samples of Zagami for this work, T. Graf for discussions, and two anonymous reviewers for constructive suggestions. We thank T. Servilla, T. Tatnall, and T. Hulsebosch for technical assistance. Supported by National Aeronautics and Space Administration grants NAGW-3428 to K.M., and NAGW-3281 to K.K. A.N.T. was supported by the California Space Grant Consortium at the University of California at San Diego. Hawaii Institute of Geophysics and Planetology publication 795 and School of Ocean and Earth Science and Technology publication 3821.

21 October 1994; accepted 9 January 1995

Crystal Structure of the β Chain of a T Cell Antigen Receptor

Graham A. Bentley,* Ginette Boulot, Klaus Karjalainen, Roy A. Mariuzza*

The crystal structure of the extracellular portion of the β chain of a murine T cell antigen receptor (TCR), determined at a resolution of 1.7 angstroms, shows structural homology to immunoglobulins. The structure of the first and second hypervariable loops suggested that, in general, they adopt more restricted sets of conformations in TCR β chains than those found in immunoglobulins; the third hypervariable loop had certain structural characteristics in common with those of immunoglobulin heavy chain variable domains. The variable and constant domains were in close contact, presumably restricting the flexibility of the β chain. This may facilitate signal transduction from the TCR to the associated CD3 molecules in the TCR-CD3 complex.

Antigen recognition by T lymphocytes is mediated by highly diverse cell-surface glycoproteins known as T cell receptors. These disulfide-linked heterodimers are composed of α and β (or γ and δ) chains consisting of variable (V) and constant (C) regions homologous to those of antibodies (*1, 2*). Although antibodies generally recognize antigens in their native form, αβ TCRs recognize antigens as peptides bound to molecules of the major histocompatibility complex (MHC) (*3*). In addition, TCRs interact with a class of molecules known as superantigens, which stimulate T cells bearing particular V_β elements (*4*). We now report the crystal structure at 1.7 Å resolution of the extracellular portion of the β chain ($V_\beta 8.2 J_\beta 2.1 C_\beta 1$) of a TCR (designated 14.3.d) specific for a hemagglutinin peptide of influenza virus [HA(110–120)] presented by the MHC class II I-E^d molecule (*5*). Production (*6*), crystallization (*7*), and structure determination (*8*) of the recombinant β chain are described below.

The TCR β chain is divided into V and C domains structurally homologous to the V and C domains of immunoglobulins (Fig. 1, A and B). The root-mean-square (rms) difference in α carbon positions is 1.4 Å with respect to V_L (compared with framework residues from nine murine V_L domains) and 1.9 Å with respect to V_H (compared with framework residues from nine murine V_H domains). The framework structure of V_β is therefore closer to that of V_L. For C_β, the structural difference with immunoglobulin homologs is greater. Sequence alignment by structural homology (Table 1) gives rms differences between 2.3 and 3.0 Å for the α carbon positions of matched residues. The C_β domain contains a large, solvent-exposed insertion with respect to other immunoglobulin C domains between residues 219 to 232 (inclusive) (Fig. 1). Sequence comparisons suggest that this insertion also occurs in C_γ domains from mice and humans. Thus, the number of amino acids between the last intrachain disulfide bridge and the interchain bridge is 34 for mouse C_β, 32 for human C_γ form 1 (*9*), 31 for mouse $C_\gamma 1$, and 26 for $C_\gamma 2$; for the immunoglobulin C_κ and $C_H 1$ domains, these are 18 and 19 residues long, respectively (*10*).

Peptide loops homologous to the complementarity-determining regions (CDRs) of immunoglobulins are disposed on the V domain to form part of the expected antigen-binding site (Figs. 1 and 2). A significant difference with respect to immunoglobulins, however, occurs in CDR1 of $V_\beta 8.2$. In both V_L and V_H domains, CDR1 is largely stabilized by the hydrophobic side chain of residue 29, which is positioned midway along this loop and oriented to intercalate between two β-pleated sheets in a nonpolar environment. By contrast, His^{29} of $V_\beta 8.2$ is displaced sideways relative to the immunoglobulin homolog and is partially exposed to the solvent (Fig. 3A). The volume occupied by residue 29 in immunoglobulin V domains is instead taken by Gln^{25} in $V_\beta 8.2$. In this configuration, the amide group of Gln^{25} stabilizes CDR1 by forming four hydrogen bonds to its main chain atoms. The CDR1 sequences of many V_β domains are similar to that of $V_\beta 8.2$ by virtue of their common length and the presence of Gln and a hydrophilic residue at positions 25 and 29, respectively. Thus, sequences listed by Kabat *et al.* (*10*) for the murine subgroup II of V_β have the same number of residues in CDR1 in which Gln^{25} and His^{29} are invariant residues. Similarly, in subgroup I Gln^{25} occurs 11 times and His^{29} occurs 35 times in 37 sequences, and all but one CDR1 have the same length. The structure described here for $V_\beta 8.2$ may therefore be common to many other V_β CDR1 structures.

Structural alignment of the $V_\beta 8.2$ domain with immunoglobulin V domains shows that the β chain CDR2 is equal in

G. A. Bentley and G. Boulot, Unite d'Immunologie Structurale (CNRS URA 359), Institut Pasteur, 25 rue du Dr Roux, 75724 Paris Cedex 15, France.
K. Karjalainen, Basel Institute for Immunology, Grenzacherstrasse 487, Postfach CH-4005, Basel, Switzerland.
R. A. Mariuzza, Center for Advanced Research in Biotechnology, University of Maryland, 9600 Gudelsky Drive, Rockville, MD 20850, USA.
*To whom correspondence should be addressed.